Supplementary Information for

SI-Nanomagnetic properties of the meteorite cloudy zone

Joshua F. Einsle, Alex Eggeman, Benjamin H. Martineau, Zineb Saghi, Sean M. Collins, Roberts Blukis, Paul A.J. Bagot, Paul A. Midgley, Richard J. Harrison

Corresponding Author Name.
E-mail: jfe26@cam.ac.uk

This PDF file includes:

Supplementary text
Figs. S1 to S13
Tables S1 to S2
Captions for Movies S1 to S11

Other supplementary materials for this manuscript include the following:

Movies S1 to S11

Supporting Information Text

Thickness Series Tomographic Quantification

S1 presents a schematic diagram showing the methodology for the thickness series tomographic unmixing. Different X-ray energy dispersive spectroscopy (EDS) signals are recorded depending on the beam trajectory and sample tilt. Volume-mixed spectra are recorded at each pixel of the tilt series depending on sample orientation. The mixed spectra recorded can be described symbolically as,

$$\Gamma_{tot}(x, y, \theta, E) = t_A(x, y, \theta)\Gamma_A(E) + t_B(x, y, \theta)\Gamma_B(E) \qquad [1]$$

where Γ_{tot} is the recorded spectral signal as a function of position (x, y), sample tilt-angle θ, and energy E. The total signal is assumed to be a linear combination of signals arising from phase A and phase B, denoted Γ_A and Γ_B. Given the thickness of each phase t_A and t_B the system of equations can be solved for the phase-specific spectra. There are then two unknowns at each energy which becomes overdetermined for more than two dissimilar trajectories. In the experimental case, many more trajectories are recorded resulting in a highly overdetermined system. The thickness map unmixing approach used here assumes the sample is adequately described as comprised of two homogeneous phases.

Additional Atom Probe Tomography Data Summary

The results of eight atom probe tomography (APT) experiments performed on various regions of the cloudy zone, tetrataenite rim and the kamacite lamella are summarized in Table S1. For the final composition of averages for the cloudy zone we do not include dataset TazeAPT05 due to large thermal tails in the mass spectra.

The raw APT data (Fig. S2) is a dense data set capturing the spatial positions of all the elemental species evaporated. It is not possible to render all of the atoms captured, so the IVAS software (3.6.12) renders a representative subset. Our method for determining the composition of the tetrataenite particles and matrix phase are schematically shown in Fig S3. By selecting cylindrical volumes that are fully contained within the selected phase this results in a more accurate determination of the pure composition of the phase, at the expense of counting statistics since smaller volumes of atoms are counted.

We present reconstructions of the APT data which are not present in the main text in Fig. S2 through S9.

Proportion of each <100> phase from SPED cluster analysis

The fuzzy means cluster analysis was performed on SPED data collected on a TEM lamella initially cut parallel to the [110] direction and tilted onto a <100> zone axis. Tilting of the lamella has the effect of increasing the effective sample thickness resulting in each pixel being a mixture of at least tetrataenite and matrix. Over 98% of the pixels in the resulting SPED orientation maps become classified as one of the three possible c-axis orientation directions. The proportion of each tetrataenite orientation are summarized in Table S2.

Kinematic Diffraction data

Ideal crystal structures for tetrataenite, and ordered Fe_3Ni were created using CrystalMaker 9. Kinematic diffraction patterns were then simulated for these ideal structures using SingleCrystal 2.3. In Fig. S10 we present the three <100> directions showing three distinct superlattice peaks associated with each unique c-axis direction. Figure S11 presets the two unique diffraction patterns and real space lattice structures for the [112] and <121> -type directions. Here, only the [112] posses unique superlattice reflections. Finally, Fig. S12 presents the diffraction data and crystal models for Fe_3Ni along the <100> and the <112> directions. Here we observe the presence of the unique <100> superlattice reflections which resemble the combination of all three <100> from tetrataenite.

Microstructural Coarsening

We present a schematic depiction of the the grain coarsening process described in the discussion of the main text in Fig. S13.

Supplemental Tables and Figures

Sample ID	CZ Region	Figure	Bulk	Volume Fraction Tetrataenite	Tetrataenite	Matrix
Taz CCZ EDS	Coarse	Fig 2, 3a	68 ± 2 Fe 32 ± 2 Ni	51.5%	52 ± 2 Fe 48 ± 2 Ni	84 ± 2 Fe 16 ± 2
Taz ICZ EDS	Intermediate	Fig 3b,c	76 ± 2 Fe 24 ± 2 Ni	28.3%	52 ± 2 Fe 48 ± 2 Ni	85 ± 2 Fe 15 ± 2
TazeAPT01 *	Coarse	S4	N/D	100%	47.5 ± 0.4 Fe 51.6 ± 0.4 Ni 0.90 ± 0.08 Co	N/D N/D N/D
TazeAPT02	Coarse	S8	N/D	100%	49.3 ± 0.3 Fe 50.5 ± 0.4 Ni 0.19 ± 0.03 Co	80.8 ± 0.3 Fe 19.0 ± 0.3 Ni 0.23 ± 0.04
TazeAPT03 *	Coarse	S5	66.93 ± 0.07 Fe 32.82 ± 0.07 Ni 0.248 ± 0.007 Co	48.11%	50.07 ± 0.05 Fe 49.71 ± 0.05 Ni 0.220 ± 0.004 Co	82.80 ± 0.03 Fe 17.04 ± 0.03 Ni
TazeAPT04	Fine	Fig 4	69.36 ± 0.02 Fe 30.1 ± 0.02 Ni 0.546 ± 0.003 Co	37.00%	48.4 ± 0.4 Fe 51.1 ± 0.4 Ni 0.60 ± 0.05 Co	81.8 ± 0.2 Fe 17.8 ± 0.2 Ni 0.47 ± 0.04 Co
TazeAPT05 **	Fine	S8	66.11 ± 0.10 Fe 27.80 ± 0.11 Ni 2.90 ± 0.04 Co	24.5%	39.0 ± 0.4 Fe 59.1 ± 0.4 Ni 1.85 ± 0.12 Co	80.8 ± 0.3 Fe 19.0 ± 0.3 Ni 2.2 ± 0.2 Co
TazeAPT06	Fine	S9	71.29 ± 0.18 Fe 27.80 ± 0.18 Ni 0.90 ± 0.04 Co	34.8%	49.3 ± 1.5 Fe 49.1 ± 1.5 Ni 1.5 ± 0.4 Co	83.0 ± 0.4 Fe 16.4 ± 0.4 Ni 0.55 ± 0.09 Co
TazeAPT07	Kamacite	S6	95.28 ± 0.02 Fe 4.16 ± 0.02 Ni 0.561 ± 0.007 Co	0%		
TazeAPT08	Tetrataenite	S6	51.11 ± 0.09 Fe 48.78 ± 0.09 Ni 0.113 ± 0.006 Co	100%	Same as bulk	

Table S1. Compositions reported in at % for each of the metallurgical phases in the Cloudy Zone (CZ) samples as well as pure kamacite and tetrataenite. The volume fraction for coarse cloudy zone is not fully representative, since in 3d-EDS and APT complete tetrataenite precipitates are not recovered. All errors reported are equal to two standard deviations based on counting statistics. All APT compositional data might be inaccurate due to excessive thermal noise in the mass spectrum.

	Tetrataenite Orientation			
Region	100	010	100	Unclassified
Coarse	52.9 %	13.9 %	32.7 %	0.4%
Intermediate	15.2 %	25.4%	58.1 %	1.2%
Fine	29.0%	28.8%	40.9%	1.3%

Table S2. Areal density of <100> SPED orientation maps for three different regions of the cloudy zone. High tilt angle makes resolving independent matrix component impossible.

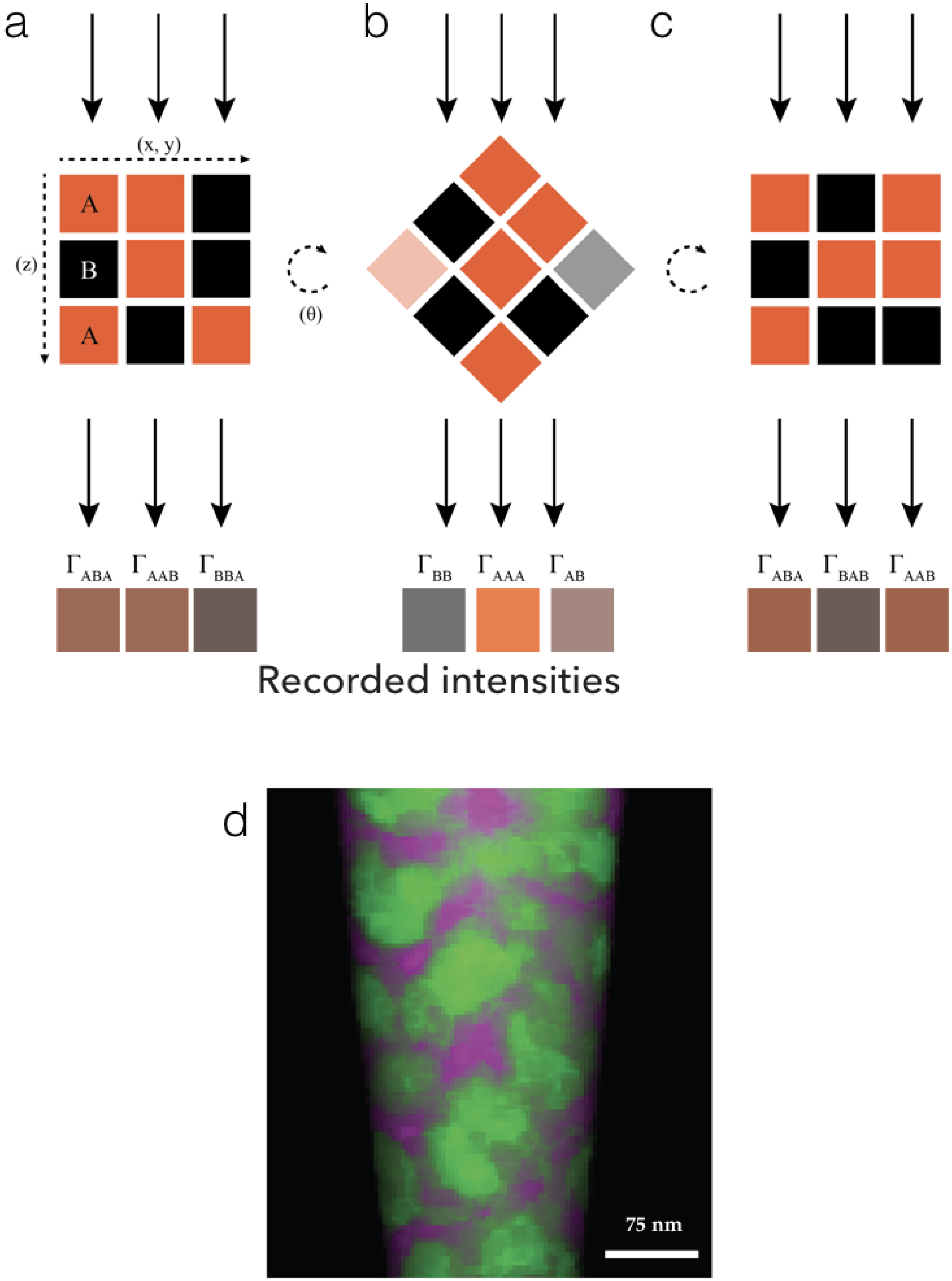

Fig. S1. Schematic depiction of the spectrographic unmixing method. a-c, Illustration of a two-phase square model object. The two phases A and B are color-coded as orange and black, respectively. The resultant spectra Γ are reasonably approximated as linear mixtures. d, A thickness map of an experimental sample, derived from segmentation of a three-dimensional volume reconstruction. Here the thickness of the two phases is coded as magenta (matrix) or green (tetrataenite).

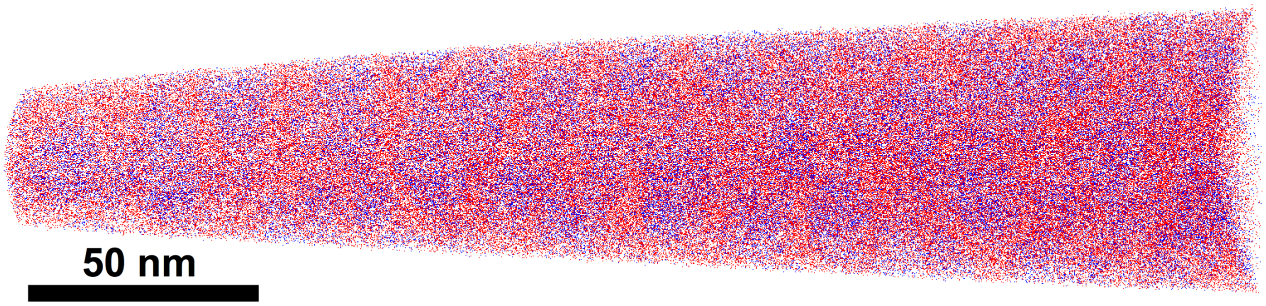

Fig. S2. A 3D output of the APT showing the positions of the detected atoms (Sample Medium CZ 1 from the table S1). The red and blue dots represent individual Fe and Ni atoms respectively. Only few % of all atoms recorded are shown to avoid clutter. Even in this raw output image clustering of Ni atoms is noticeable.

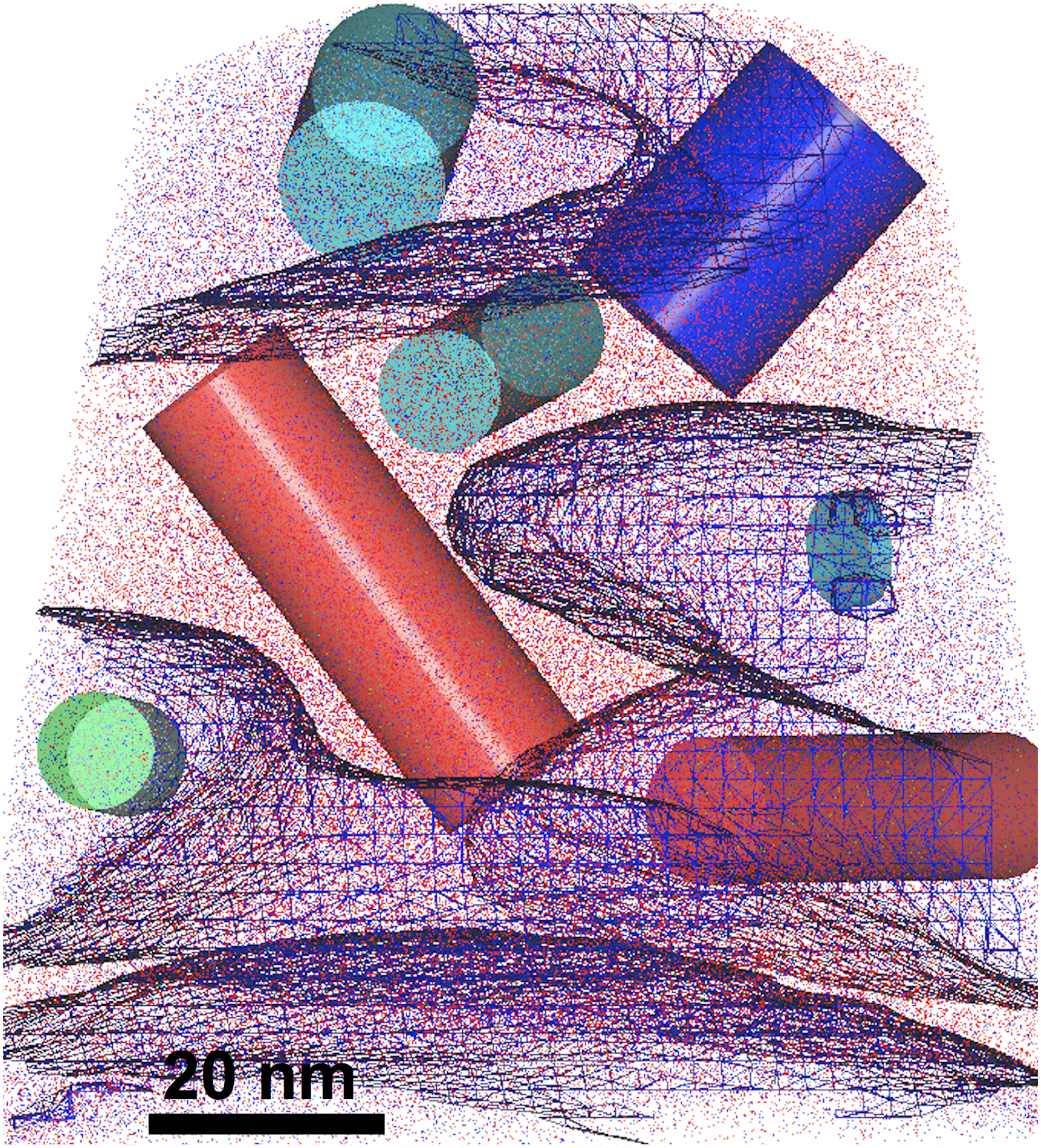

Fig. S3. An example of cylindrical ROIs placed inside the tetrataentite particles and the matrix for composition determination. The wire mesh represents 41 at% Ni isosurface and shows the edges of the tetrataenite particles. This is a sample of a coarse cloudy zone (sample Coarse CZ 3 in table S1).

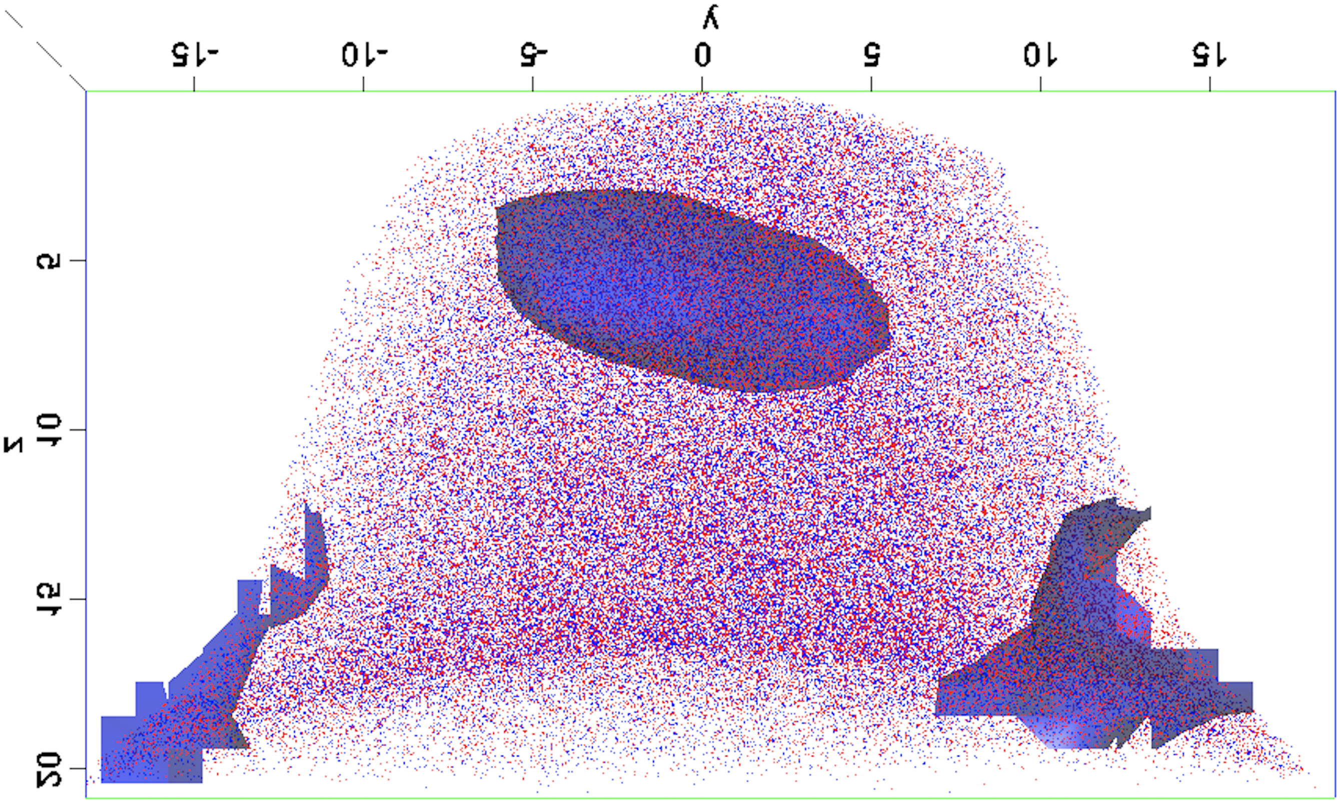

Fig. S4. Small region of the coarse cloudy zone studied using 3D-EDS. Due to oxidation, tip fractured shortly after evaporation began. However, it is possible to observe the presence of a secondary precipitate in the large tetrataenite island captured in the reconstitution (sample TazeAPT1 in table S1). Isosurfaces are shown at 32.5 at% Ni concentration.

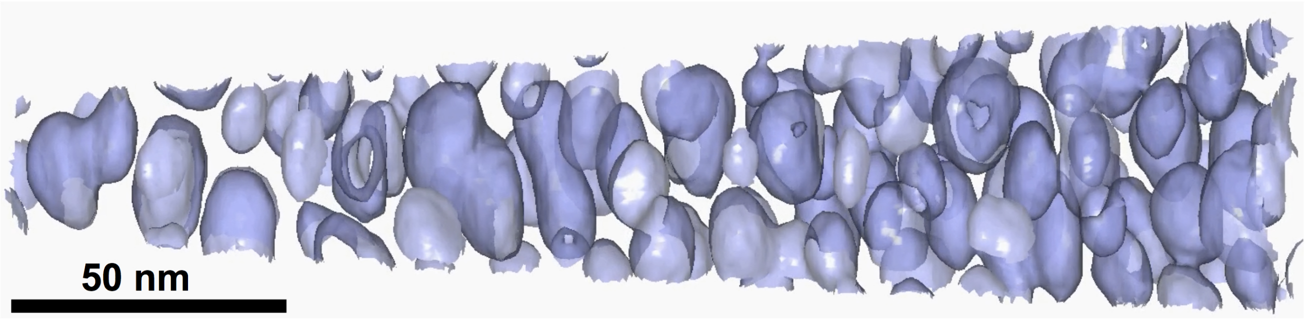

Fig. S5. A sample of the medium cloudy zone. Only 44 at% Ni isosurface is shown marking the locations and shapes of the tetrataenite particles. This sample corresponds to sample Medium CZ 1 in the table S1.

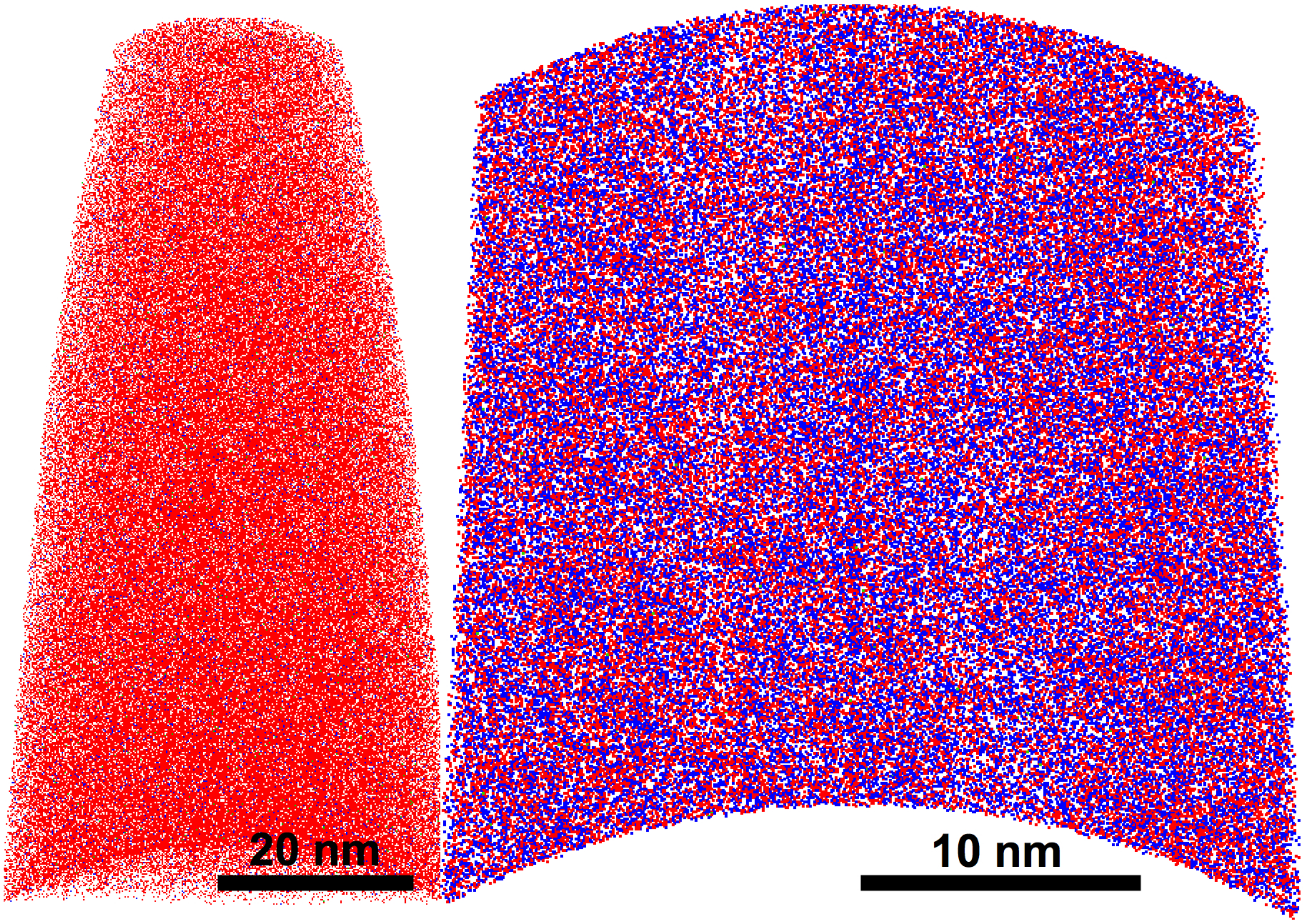

Fig. S6. Samples of pure kamacite (left) and tetrataenite (right). Kamacite is shown as a raw output with dots representing atoms in the whole volume of the needle. Tetrataenite sample is shown a 1.5 nm thick slice with all atoms detected shown. Red, blue and green dots represent Fe, Ni and Co atoms respectively. Vertical features of higher and lower atom density in the tetrataenite indicate the sample has been well aligned along a crystallographic pole, (100) in this case.

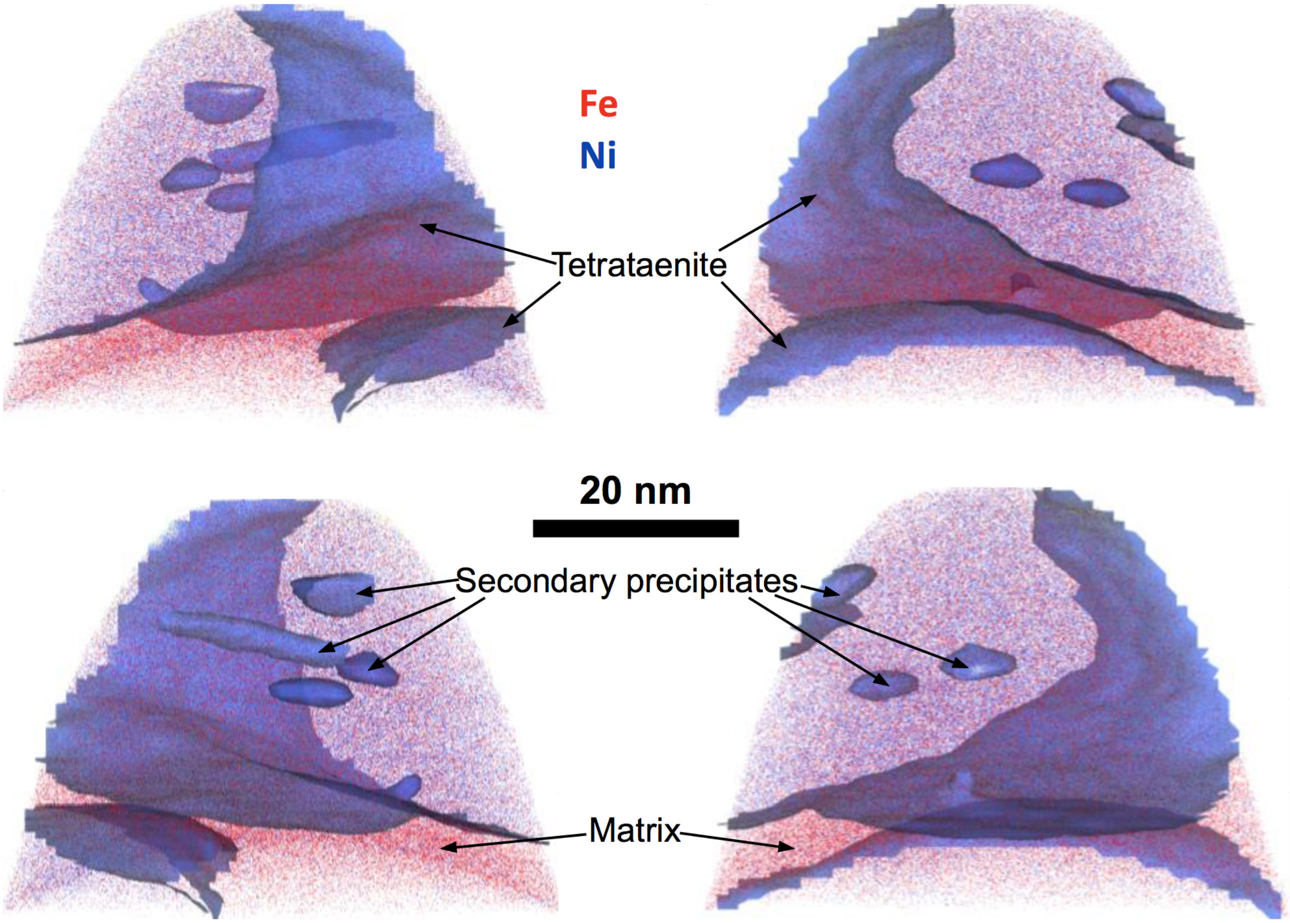

Fig. S7. A sample of the coarse cloudy zone shown from 4 different viewing angles at right angles to each other. The sample captures parts of two tetrataenite particles. 7-12 nm thick layer of matrix separates the two islands in the lower part of the sample. Secondary precipitates can be seen inside the upper tetrataenite particle. Red and blue dots represent Fe and Ni atoms respectively. The isosurface is drawn at 37.5 at% Ni. This sample corresponds to sample Coarse CZ 2 in the table S1.

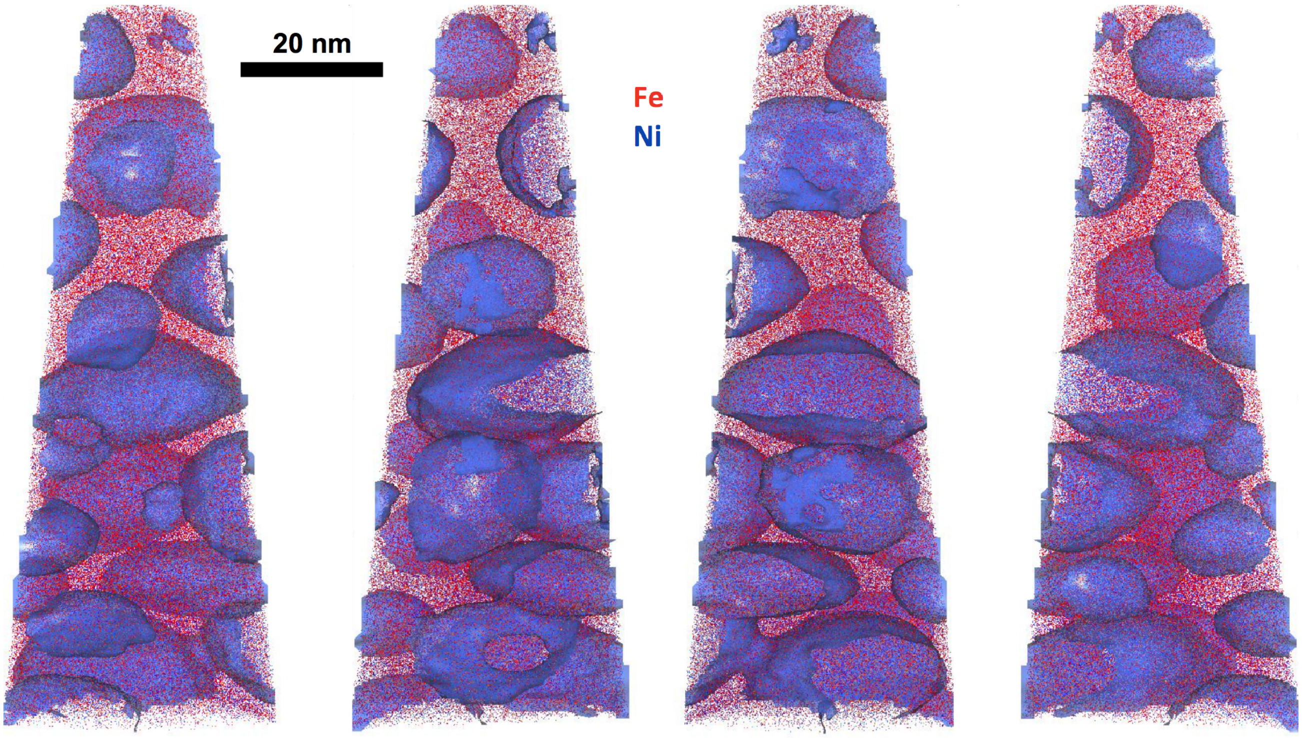

Fig. S8. A sample of the medium cloudy zone shown from 4 different viewing angles at right angles to each other. Secondary precipitates were not detected in this sample. Red and blue dots represent Fe and Ni atoms respectively. The isosurface is drawn at 37 at% Ni. This sample corresponds to sample Medium CZ 2 in the table S1.

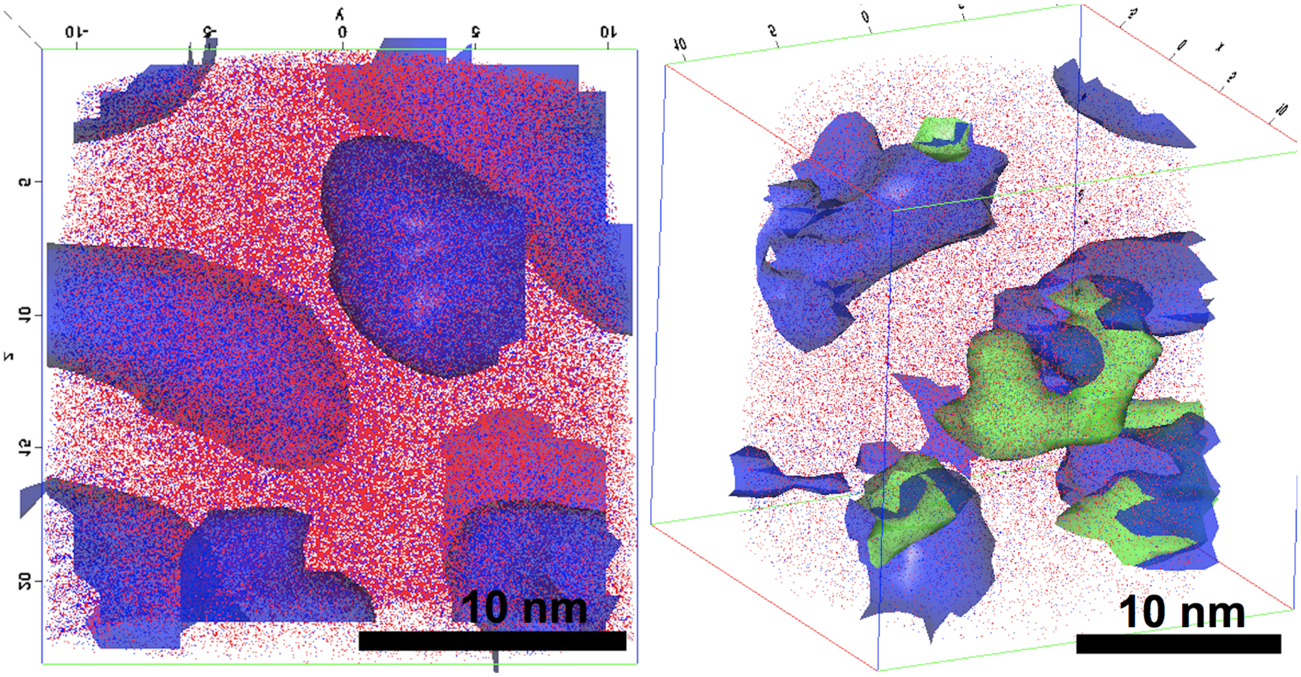

Fig. S9. A sample of the fine cloudy zone showing 5-10 nm size particles with 40.4 at% Ni isosurface shown (left). 45 at% Ni isosurface (blue) combined with 2 at% Co isosurface (green) (right). Red, blue and green dots correspond to Fe, Ni and Co atoms respectively.

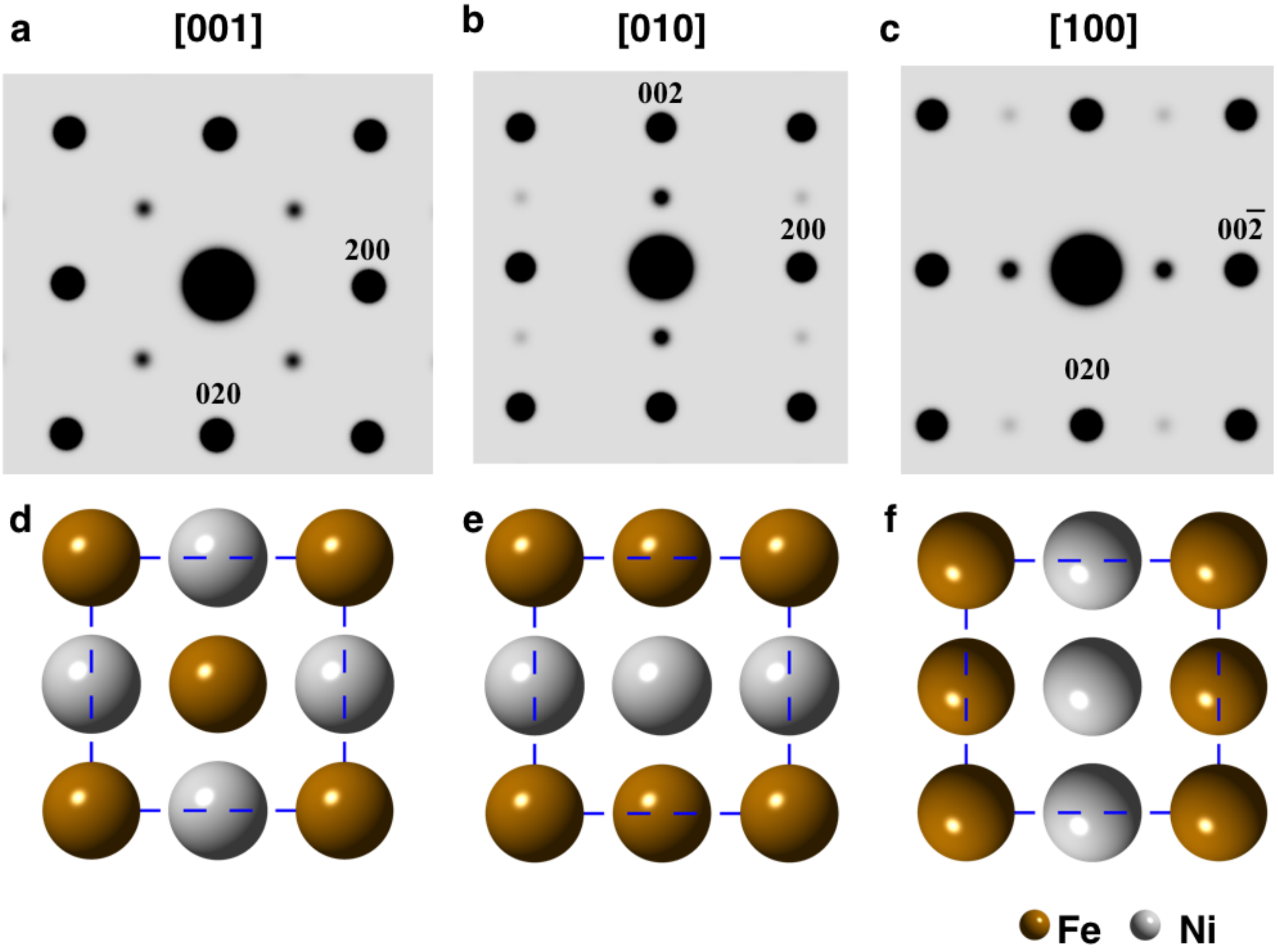

Fig. S10. Kinematic diffraction patterns and model structures for tetrataenite when viewed along the three principle crystallographic directions, <100>.

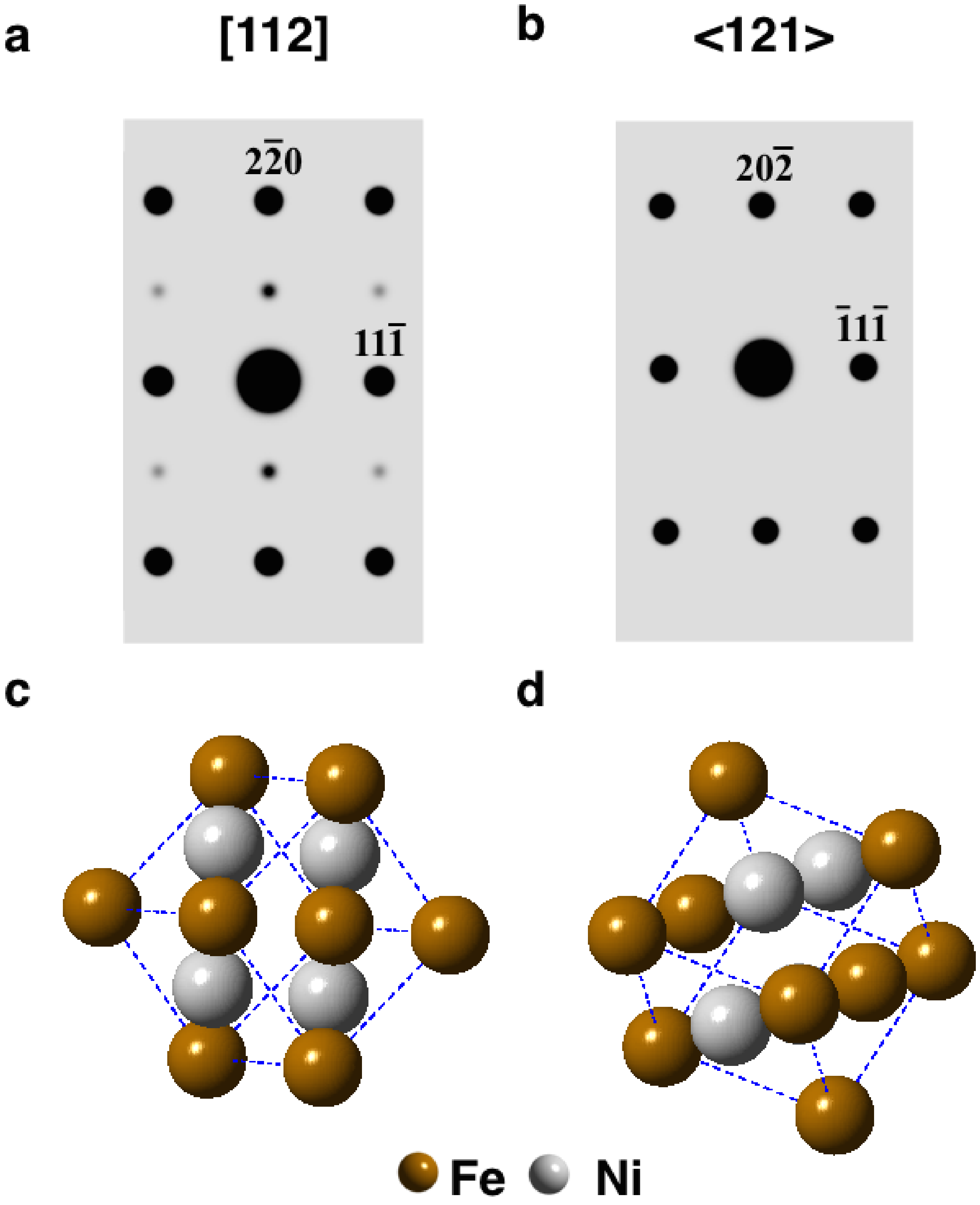

Fig. S11. Kinematic diffraction patterns and model structures for tetrataenite when viewed along the [112] or the <121> (this includes the [121] and [211]-like directions.

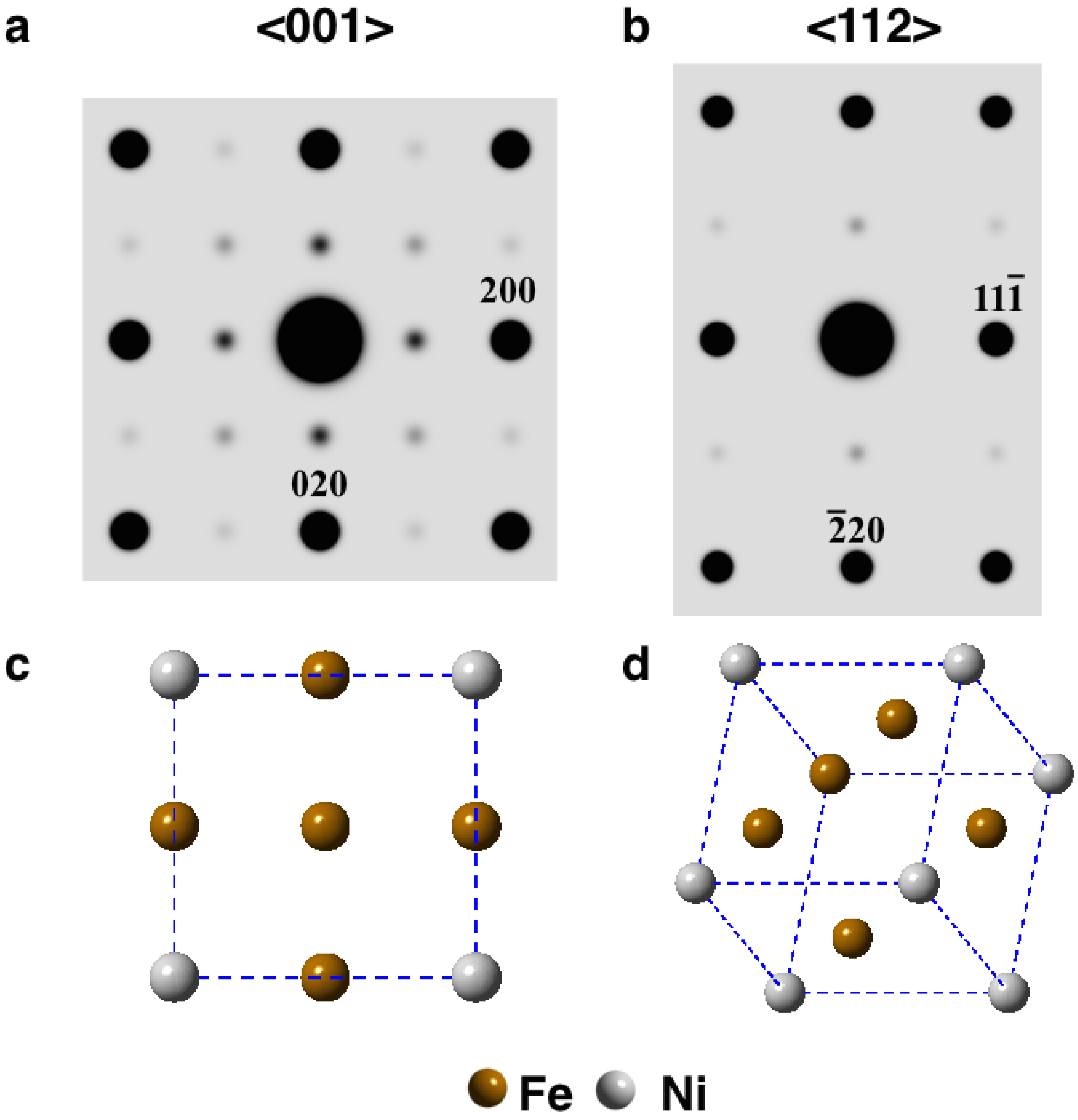

Fig. S12. Kinematic diffraction patterns and ideal structures for Fe_3Ni when viewed along the principle crystallographic directions, <100>, as well as the <121> directions. Due to the symmetry of the $L1_2$ structure there is one pattern for each of the two families of directions.

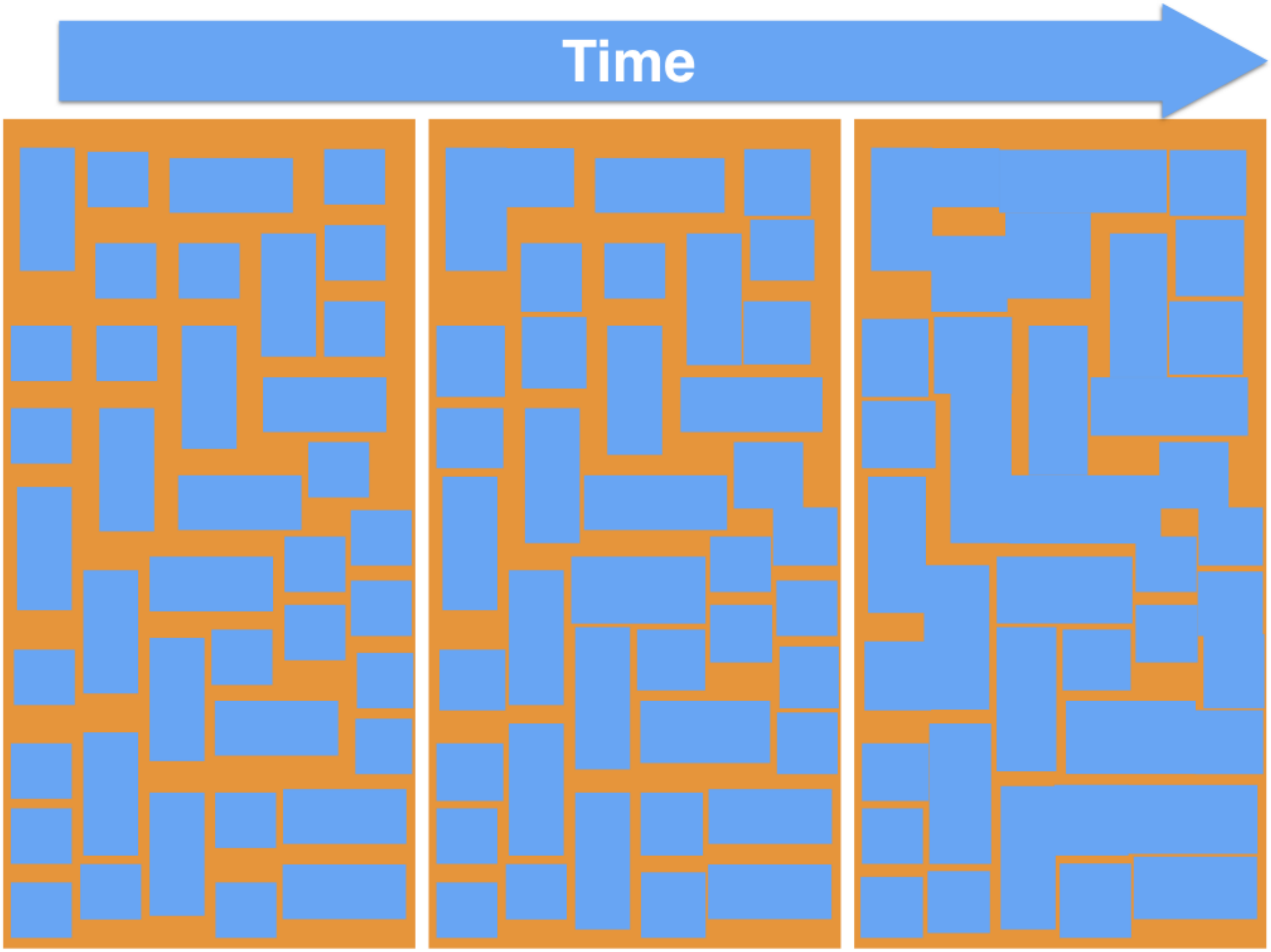

Fig. S13. Schematic drawing showing grain coarsening process of the cloudy zone as a function of time.

Movie S1. Volume render of nickel concentration of the coarse cloudy zone. (Arbitrary units)

Movie S2. Volume render of nickel concentration of the medium cloudy zone. (Arbitrary units)

Movie S3. Proxigram showing isosurfaces defined by 32.5 at % Ni content in the fine cloudy zone. Upper half of APT data set collected.

Movie S4. Proxigram showing isosurfaces defined by 32.5 at % Ni content in the fine cloudy zone. Lower half of APT data set collected.

Movie S5. Volume mesh for three particles extracted from the medium cloudy zone.

Movie S6. Hysteresis behavior for the red particle in S5 simulated individually. These depict the magnetic behavior as the uniaxial anisotropy was set to the major (left), intermediate (center), and minor axis of the particle. These start at the remanence state and proceed towards saturation.

Movie S7. Hysteresis behavior for the white particle in S5 simulated individually. These depict the magnetic behavior as the uniaxial anisotropy was set to the major (left), intermediate (center), and minor axis of the particle. These start at the remanence state and proceed towards saturation.

Movie S8. Hysteresis behavior for the blue particle in S5 simulated individually. These depict the magnetic behavior as the uniaxial anisotropy was set to the major (left), intermediate (center), and minor axis of the particle. These start at the remanence state and proceed towards saturation.

Movie S9. Hysteresis behavior for the thee particles simulated together as non-interacting (left) and interacting particles (right) starting from the remanence state and proceeding towards saturation.

Movie S10. Movie showing the change in magnetic state as the particles changes from the high temperature taenite to low temperature tetrataenite.

Movie S11. Movie showing the motion of a sharp domain wall in response to the applied magnetic field.